# A Theoretical Feedback Control Scheme for the Ultrasound-Assisted Continuous Antisolvent Crystallization of Aspirin in a Tubular Crystallizer

Symeon V. Savvopoulos,[†] Spyros S. Voutetakis,[‡] Simon Kuhn,[†] and Dimitris Ipsakis*,[¶]

[†]*KU Leuven, Department of Chemical Engineering, Celestijnenlaan 200F, 3001 Leuven, Belgium*

[‡]*Chemical Process and Energy Resources Institute, Centre for Research and Technology Hellas, 57001 Thermi, Thessaloniki, Greece.*

[¶]*Industrial, Energy and Environmental Systems Lab, School of Production Engineering and Management, Technical University of Crete, 73100 Chania, Greece.*

E-mail: dipsakis@pem.tuc.gr

Phone: +30 28 21 03 73 62

**Abstract**

Ultrasound-assisted crystallization is a promising process for the production of crystals within a size distribution width. Towards the direction of attaining high-quality crystals, this article proposes and assesses a theoretical feedback control scheme that can be applied in a continuous tubular crystallizer. In this crystallizer, the antisolvent crystallization of aspirin (pharmaceutical ingredient), in water (antisolvent), and

1

ethanol (solvent) takes place under ultrasound. Initially, a dynamic model is developed and includes the aspirin's concentration variations while also taking into account temperature modifications in the inlet. After model validation, a PI control scheme is finely tuned, implemented theoretically and critically assessed at the i) the trajectory control of the crystal length (average size), ii) the alleviation of suddenly emerged disturbances (e.g., solvent flow rate, inlet temperature), and iii) combination of worst-case operating scenarios. As was identified, the proposed controller can offer a practical platform that can be readily applied to different scales and geometries in continuous tubular crystallizers operating with ultrasound. During all simulations, the produced crystals maintained a high-quality.

**keywords:** control, antisolvent crystallization, ultrasound, *in silico*, dynamic model, continuous operation

# 1 Introduction

Crystallization is used at an industrial scale for the organic nano and microparticle production. The produced crystals can be active as pharmaceutical ingredients (APIs) and nanodispersions, both useful in dyeing and pharmaceutical industry.[1] Currently, batch crystallization is still applied in large industrial units due to the amount of equipment and related studies focused on it. However, it has shown limitations regarding heat and mass transfer issues. These limitations render batch processes less flexible, costly, and less controllable.[2] Furthermore, batch-to-batch variation invokes a further complication, as the product quality is affected, whereas the large size of the crystallizers invokes increased operating and maintenance cost. For these reasons, lead researchers to investigate the concept of optimizing the cost and the efficiency of the continuous crystallization processes.[2] Specifically, modification that can be dynamically applied to the operating conditions can be quickly adopted via controlling certain characteristics of the crystals, such as the average particle size, the particle size distribution (PSD), and the particle's shape.[3,4] To this end, continuous crystallization

is in the spotlight nowadays, as it has revealed significant advantages as compared to the conventional batch processes.[1]

The API used in this work is aspirin (acetylsalicylic acid - ASA), which is used worldwide,[5] whereas, ultrasound is selected to control the particle size and the crystals' size distribution. Apart from pharmaceutics, ultrasound is used in food processing for size and shape control, as well.[6] With this combination, it has been confirmed that the cavitation bubbles are responsible for generating a new nucleation site, breaking larger crystals, and reducing the induction time that leads to the production of small-sized crystals with a narrow PSD.[7–10] The main novelty that this study aims to provide is to develop and assess theoretically a feedback control scheme based on conventional controllers (e.g., PID or PI) that will be possible to be readily applied to the on-going lab-scale setup. In this way, an advanced set of suitable operating conditions will be extracted towards producing small crystals under suddenly emerged disturbances. To the best of the authors' knowledge, only a limited number of studies have focused on the feedback control of the aspirin's ultrasound-assisted continuous antisolvent crystalization. Eder et al. tried to control the mean diameter of crystals by varying seed loading and applying a temperature cycle strategy.[11] With this formulation, a certain length of crystals was obtained, but without considering the effect of disturbances or set-point modifications. Tokuhisa et al. studied the operation of a microscale device where the temperature was the main controlled variable that was regulated towards achieving desired crystals.[12] In a rather concrete study, Nagy et al. reviewed several crystallization processes from the perspective of monitoring and control.[13] Among their outcomes, the development and application of advanced feedback control systems were categorized as a significant key pole towards reaching a mature operating stage for batch crystallization systems. Earlier to this study, Fujiwara et al. presented a model-based approach for the effective control design and application of pharmaceutical crystallization.[14] As was found, the need for accurate models is important in order to design suitable feedback control schemes. A rather interesting approach was also presented by Kwon et al.[15] There, a feedforward

controller was applied towards crystal shape and size and with an aim to alleviate emerged disturbances. Last but not least, Diab and Gerogiorgis optimized the operating conditions for Melitracen production with the use of a techno-economic mixed integer nonlinear programming optimization of mixed suspension, mixed product removal crystallizer cascades.[16]

Following the above progress on modeling and control of crystallization systems for aspirin-based applications, two main issues need to be tackled. The first is the proper and accurate dynamic modeling of the ultrasound-assisted continuous antisolvent crystallization. The second is the identification of suitable control schemes that will be able to maintain a high-quality of crystals within the underlined process. Especially, the on-going progress of control schemes should lie on the following rules: (1) development of a high-fidelity process model, (2) coupling feedback controllers to the complex process, (3) estimating the critical parameters of the controller with proper tuning methods and (4) "closed-loop," in-silico validation of the controller against the process model. The lab-scale experimental setup that is used as the basis of this theoretical assessment, consists of a tubular crystallizer in a cooling bath and an ultrasound transducer located underneath the crystallizer. Our lab-scale experimental setup was validated mathematically in a previous work by using a nonlinear high fidelity model.[17,18] Specifically, antisolvent crystallization occurred within the crystallizer under sonication.[17,18] These types of tubular crystallizers are compact and can easily produce the desired quantity of an API. Moreover their acoustic field is more uniform along the crystallizer, and can be used for the necessary scale-up.[19] The high fidelity model contained population balance modeling (PBMs) equations because these equations can capture the number and size of the crystals during the process.[20]

As can be revealed, controlling the average crystal size under disturbances is quite a challenging process. Towards this direction, this article's core objective is to theoretically develop and assess a conventional feedback controller for the ultrasound-assisted continuous antisolvent crystallization of aspirin. Diverging from previous studies that control the continuous antisolvent crystallization processes, this article presents a simplified, yet accurate,

4

controller scheme that (1) considers disturbances in the API inlet concentration and the inlet temperature (taking into consideration different profiles of disturbances) , (2) considers disturbances in the solvent flow rate, and (3) controls the trajectory of the volume based mean crystal size. This study aligns with the on-going efforts for optimizing continuous crystallization processes, assessing advanced control schemes and finally for the realistic control implementation in the lab operating unit, which is the next step in this research area.

# 2 Proposed Experimental Setup, Mathematical Modeling, and Control

## 2.1 Experimental Setup

Before proceeding to the theoretical section of this study, it is necessary to add a brief description of the proposed experimental setup shown in Figure 1.[17,18] The main lab-scale experimental setup consists of a tubular crystallizer and an ultrasound transducer that operates at 24 W and 42 kHz, and is located underneath the crystallizer. Antisolvent crystallization occurs within the crystallizer under sonication.[17,18] The productivity of the setup ranges from 130 to 240 mg/min. As long as the system runs dynamically, the additional units refer to a high-speed camera accompanied by a sensor and a controller.

The tubular crystallizer was selected because these kinds of crystallizer can produce a desired quantity of an API easily, whereas, the acoustic field is more uniform along the crystallizer. The system is water-cooled in order to keep the temperature fairly constant due to the ultrasound. Crystals are measured offline and at high residence time when steady-state conditions have been achieved.[17] As can be seen in Fig. 1, there are two main inlets, a) the upstream solution inlet that contains the ethanol with the API and b) antisolvent (water). These two streams are mixed before the ultrasound transducer inlet. The increased water weight fraction in the mixture and the cavitation bubbles initially induce the nucleation and

then the crystal growth.

The ultrasound transducer increases the temperature of the mixture by 3-5$^o$C along with the crystallizer. Both nucleation and growth rate depend on temperature and the concentration of the API within the crystallizer. The crystals at the outlet cross the cell of a high-speed camera for characterization. Specifically, the crystals pass through a thin flow cell in the optical path during their movement. A beam of light passes through the flow cell and in this way the images of the particles are projected onto a high-resolution camera sensor.[21,22] The controller sampling time can be pre-selected at 10 s, which is a generally accepted time when a physicochemical phenomenon is not expected to vary significantly through this time period. Clearly, the proposed process proceeds in a time scale of several minutes and hence this 10 s sampling time is considered an accurate selection and really close to the process residence time.

The measured volume-based mean crystal size controls the antisolvent's flow rate in the experimental setup with the aid of a valve under disturbances. As disturbances are of concern, the inlet concentration in the upstream, and the inlet temperature can be considered. After their route from the high-speed camera, the crystals are collected in a beaker. Based on this experiment setup, the main controlled variable of the system is the volume-based mean crystal size, whereas the manipulated variable is considered to be the antisolvent flow rate. Under the presented experimental setup, this study can evaluate a feedback controller's application towards high-quality crystals production theoretically. The controller's assessment is based on the developed mathematical model that is presented in the next section.

## 2.2   Mathematical Model

Dynamic population balance models (PBMs) of crystallization are used. Their most crucial part is the number and size of the crystals that are captured during the process. Overall, the mathematical model of the ultrasound-assisted continuous antisolvent crystalization of aspirin in a tubular crystallizer consists of the following group of equations: a) the population
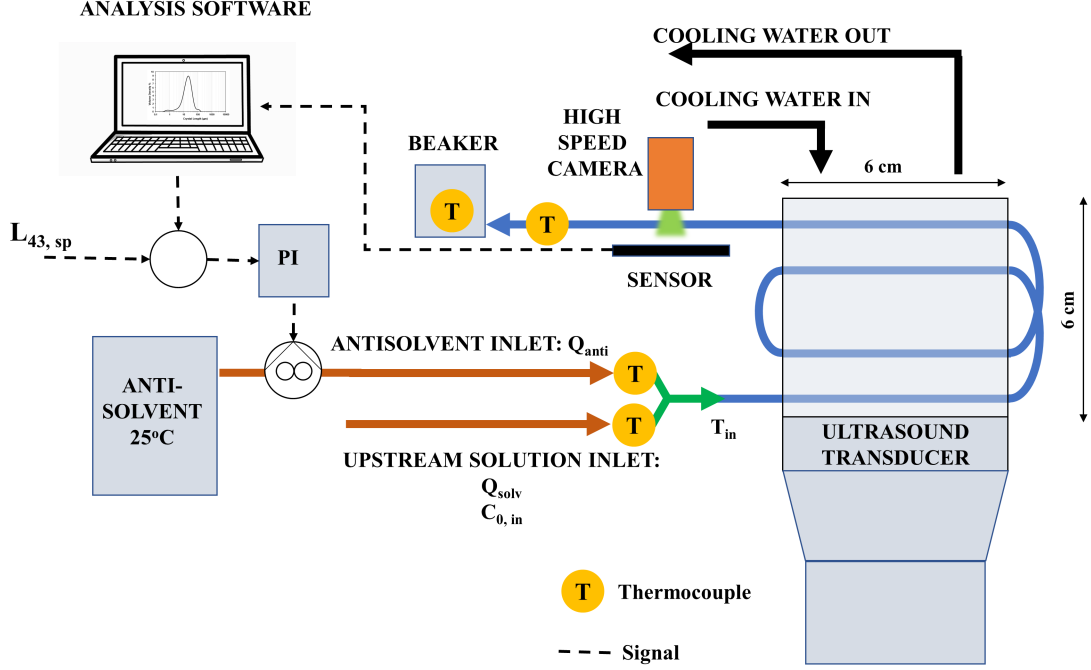
Figure 1: Proposed experimental setup for controlling the crystal average size under disturbances during the antisolvent crystallization of aspirin (adapted from[17]).

density of the crystals, b) the mass balance of the API, and c) the energy balance.

The population density of the crystals along the tubular crystallizer is given by:[23]

$$\frac{\partial n}{\partial t} + \frac{\partial (v_z n)}{\partial z} + \frac{\partial (Gn)}{\partial L} = 0 \tag{1}$$

where $n$ is the number probability density function of crystals in the slurry [#/($\mathrm{m}^3$ m)], $t$ represents the time [s], $v_z$ is the slurry velocity along the crystallizer [m/s], $z$ is the axial position in the crystallizer [m], $G$ is the crystal growth rate [m/s], and $L$ is the characteristic crystal length [m]. The velocity of the slurry $v_z$ is calculated from:

$$v_z = \frac{4(Q_{solv} + Q_{anti})}{\pi d_{in}^2} \tag{2}$$

where $Q_{solv}$ represents the volumetric flow rate of the solvent with the solute [$\mathrm{m}^3$/s], $Q_{anti}$ is the (manipulated variable) volumetric flowrate of the antisolvent [$\mathrm{m}^3$/s], and $d_{in}$ is the inner diameter of the channel [m].

The solute mass balance is:

$$\frac{\partial C}{\partial t} + \frac{\partial (v_z C)}{\partial z} + 3\rho_c K_v \int GL^2 n dL = 0 \tag{3}$$

where $C$ represents the concentration of the aspirin in the solution [kg/m³], $\rho_c$ is the crystal density which equals 1400 kg/m³, and $K_v$ is the volumetric shape factor of a crystal and equals to 1 [-], denoting that the crystal shape is cubic.

The energy balance is:[15]

$$\frac{\partial T}{\partial t} = -v_z \frac{\partial T}{\partial z} - \frac{U_c a_c}{\rho C p}(T - T_w) + \frac{P_{net,cal}}{\rho C p} + \frac{\Delta H_{crys}}{\rho C p} \tag{4}$$

where $T$ represents the temperature [K], $T_w$ is the wall temperature that is affected by cooling water [K], $U_c$ is the overall heat transfer coefficient which equals to 150 J/(m² s K),[24] $a_c$ is the heat transfer area per unit volume $(4/d_{in})$[15] [m²/m³], $Cp$ represents the mixture specific heat capacity which equals to 4130 J/(kg K),[25] $\rho$ is the mixture density which equals to 945 kg/m³,[26] $\Delta H_{crys}$ is the heat of crystallization [W/m³] which is considered negligible,[27] and $P_{net,cal}$ is the calorimetric power of ultrasound [W/m³], which is estimated at:[17]

$$P_{net,cal} = 66230.5\, P_{net,US} \tag{5}$$

where $P_{net,US}$ is the applied ultrasound power [W].

The number density $n$, the solute concentrations $C$, and the energy balance are given by partial differential equations; thus, they are functions of the crystallizer axial position $z$ and time $t$. The boundary conditions of Eqs. 1, 3, and 4 are:

$$n(L_0 = 0, z, t) = \frac{B_{son}}{G} \tag{6}$$

$$n(L, 0, t) = n_{feed}(L, t) \tag{7}$$

$$C(0, t) = C_{0, in} \frac{Q_{solv}}{Q_{solv} + Q_{anti}} \tag{8}$$

$$T(0, t) = T_{in} \tag{9}$$

where $B_{son}$ is the sonicated nucleation rate $[\#/(\mathrm{m}^3\,\mathrm{s})]$, $L_0$ is the nuclei size $[\mathrm{m}]$ ($L_0 = 0$ m for unseeded crystallization), $n_{feed}$ is the crystal size distribution at the inlet of the crystallizer (which should be known in a seeded crystallization, or in a feed supplied slurry from an upstream process) $[\#/(\mathrm{m}^3\,\mathrm{m})]$, and $C_{0, in}$ is the initial solute concentration dissolved in the upstream process. As for the energy balance, $T_{in}$ is the inlet temperature $[\mathrm{K}]$ whose value is a combination of the temperature of the upstream process, and the heat of mixing between the water and the ethanol.[17,18,28]

Furthermore, the initial conditions of Eqs. 1, 3, and 4 are:

$$n(L, z, 0) = n_0(L, z) = 0 \; \#/(\mathrm{m}^3 \, m) \tag{10}$$

$$C(z, 0) = C_0 = 0 \; kg/m^3 \tag{11}$$

$$T(z, 0) = T_0 = 298K \tag{12}$$

where $n_0$ and $C_0$ are the initial number probability density function for the PSD and the initial API concentration in the crystallizer, respectively, and $T_0$ is the initial temperature.

The supersaturation ratio $S$ [-] is defined as:

$$S = \frac{C_w}{C_{sat}} \tag{13}$$

where $C_w$ is the aspirin concentration in [kg/kg], and $C_{sat}$ is the solubility of the API. More information have been included in the work of Savvopoulos et al.[17]

The crystallization can be modeled by the use of empirical expressions as Schall et al.,[29] and Bari with Pandit[30] followed. In our setup, the sonicated nucleation rate consists of the nucleation caused by ultrasound, $B_{ultr}$ and secondary nucleation, $B_{sec}$. When $S > 1$, the sonicated nucleation rate is:[17]

$$
\begin{aligned}
B_{son} &= B_{ultr} + B_{sec} \\
B_{ultr} &= k_{j1,\,son} \exp\left(\frac{k_{j2,\,son}}{RT}\right) \exp\left(-\frac{k_{j3,\,son}}{ln^2 S}\right) \\
B_{sec} &= k_{sec,\,1} \exp(-k_{sec,\,2} w)(S-1)^2 \mu_2
\end{aligned}
\tag{14}
$$

where $k_{j1,\,son}$ [#/(m$^3$ s)], $k_{j2,\,son}$ [J/mol], $k_{j3,\,son}$ [-], $k_{sec,1}$ [#/(m$^2$ s)] and $k_{sec,2}$ [-] are all empirical parameters, $R$ is the universal gas constant 8.314 J/(K mol), and $\mu_2$ is the second moment of $n$ [m$^2$/m$^3$], estimated as:

$$\mu_2 = \int L^2 n \, dL \tag{15}$$

The empirical parameters used here affect the nucleation rate's evolution at different temperatures and supersaturation ratio values.

The growth rate when $S > 1$ is:[31]

$$G = k_{G1} \exp\left(-\frac{k_{G2}}{RT}\right)(C_{sat}(S-1)) \tag{16}$$

where $k_{G1}$ [m/s] and $k_{G2}$ [J/mol] are empirical parameters that affect the crystal growth rate

at different supersaturation ratios $S$ and temperatures $T$.

The mathematical model that was discussed in this section was developed according to certain assumptions. First of all, ultrasound increases the nucleation rate. Su et al. optimized an unseeded antisolvent crystallization process, as well.[23] In their model, agglomeration, breakage, and attrition terms were removed in Eq. 1. The tubular crystallizer's inner diameter is small, something that eliminates significant radial concentration or temperature gradients. Lastly, the inlet API concentration changes dynamically with the inlet flowrates' variations (Eq. 8). Though, inside the crystallizer, there is a dynamic turbulent micromixing, which is caused by the cavitation bubbles generated from the ultrasound. Therefore, incorporating the dilution variation by the dynamic system's inlets could be quite complex and beyond this research. For simplicity, the antisolvent content in the crystallizer's inlet could be considered the same along its axial length due to the turbulent micromixing.

### 2.2.1 Solution of PBMs

In order to solve the PDEs of the system dynamically, all the PDEs need to be discretized along the z- and L- axis in $n_z$ and $n_L$ bins, respectively. This discretization will generate a large number of Ordinary Differential Equations (ODEs) that will make the solution of the modeling set computationally expensive. More precisely, the crystallization model consists of $n_z \cdot n_L + 2 \cdot n_z$ ODEs with their initial conditions (polulation density, temperature, and concentration), 6 algebraic equations including boundary conditions and the antisolvent content. Also, there are $9 \cdot n_z + n_L$ discretized algebraic equations including the API solubility which changes along z-axis. The number of variables is $2 \cdot n_z \cdot n_L + 13 \cdot n_z + n_L + 13$ (with initial conditions). The assigned variables are mentioned in section 2.2. Instead of discretization, the method of moments is proposed for this study.[23] The $k^{th}$ moment of the system is defined as:

$$\mu_k = \int L^k n dL, k = 0, 1, ..., 5 \tag{17}$$

Based on the classical method of moments (MOMs), the PDEs can be integrated along

the crystal length L by conversion into a set of moment ODEs, and the computational cost is reduced significantly. Using the MOMs, the moment transformation of the PDEs into the first five moments are:

$$\frac{\partial \mu_0}{\partial t} + \frac{\partial (v_z \mu_0)}{\partial z} = B_{son} \tag{18}$$

$\forall\ k \in \{1,2,...,5\}$

$$\frac{\partial \mu_k}{\partial t} + \frac{\partial (v_z \mu_k)}{\partial z} = kG\mu_{k-1} \tag{19}$$

In Eqs 18 and 19 the upwind discretization scheme was applied to the crystallizer's axial position z.

Therefore, the volume-based mean crystal size is:[23]

$$L_{43} = \frac{\mu_4}{\mu_3} \tag{20}$$

and the coefficient of variation is:[23]

$$CV = \sqrt{\left( \frac{\mu_3 \mu_5}{\mu_4^2} - 1 \right)} \tag{21}$$

with the use of the MOMs, the model consists of $8 \cdot n_z$ ODEs with their initial conditions, 7 algebraic equations and $10 \cdot n_z$ discretized algebraic equations along z- axis. The number of variables is $27 \cdot n_z + 13$ (with initial conditions), which plenty of them are assigned in section 2.2.

## 2.3  Development of a Feedback Control Scheme

Based on the above-mentioned mathematical model, the proposed feedback control system is shown in Figure 2. The control framework includes 4 distinct steps briefly stated here, and discussed in more detail in section 3.

The first step refers to the model development and its validation. The model's quality affects all the other steps needed for completing the control and hence, should be developed

as accurate as possible. The "heart" of the second step is the high fidelity model developed previously (section 2.2). The high fidelity model is simplified with the use of MOMs. The new form of the model contains partial differential equations (Eqs. 18 and 19) and algebraic equations of high complexity (e.g., the nucleation and growth rates). As was shown, this group of models is discretized in tubular axial position z, and a set of differential equations is generated. During the coupling of the feedback controller, there is no kind of model reduction and system identification of the MOMs model. Therefore, the control is applied to the MOMs model in MATLAB software directly. In the third step, the high fidelity model (the process in Fig. 2) is coupled with the feedback controller and used. The controller was applied in the known velocity form (discretized with a sampling time $T_s$). The block diagram of the process studied is represented in Fig. 2.

The error is calculated as the difference:

$$e = L_{43,\,sp} - L_{43} \tag{22}$$

where $L_{43,\,sp}$ represents the set-point of the $L_{43}$.

The overall PID control function is:[32]

$$p = K_c\Big(e + \frac{1}{\tau_I}\int ed\tau + \tau_D\frac{de}{dt}\Big) \tag{23}$$

where $K_c$ is the proportional term, $\tau_I$ is the integral time, and $\tau_D$ is the derivative time.

In order to obtain the suitable controller parameters, the Ziegler-Nichols tuning is applied since it has its suitability in continuous processes.[33,34] The proportional controller gain ($K_C$ value) is gradually increased until oscillations of a constant magnitude are identified. Next, the suitable controller parameters (P or PI or PID) are estimated via known table correlations. If needed, fine-tuning is conducted until an acceptable behavior in the model output is achieved.[35] The predefined step of tuning is included thoroughly in the Supplementary Material, where a PI controller was eventually selected (section 3). In our model,
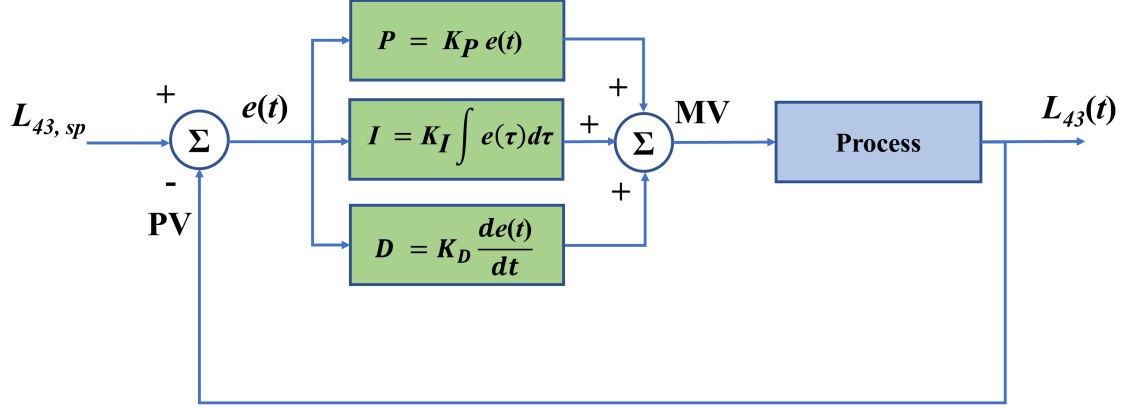
Figure 2: The block diagram of the PID controller in a feedback loop. $L_{43, sp}$ is the desired process value or set-point (SP) in the volume-based mean crystal size, and $L_{43}$ is the measured process value (PV). The manipulated variable (MV) in our system is $Q_{anti}$

we discretized the z-axis in 100 bins, and the time needed for applying control was roughly 2 minutes. The discretization in L- axis is neglected with the use of MOMs.

# 3    Results and discussion

## 3.1    Step 1. Modeling and Simulation.

The high fidelity model is originally published by Savvopoulos et al.,[17] which is based on the previous experimental work of Hussain et al.[18] Briefly, experiments with varying conditions were performed in the sonicated milifluidic crystallizer. In this way, the process model which consists of population balance modeling equations could be developed.[17,18] The parameters of the model that were obtained from a maximum likelihood estimator method through gPROMS,[36] allowed the model to predict (model validation) the crystal growth and the production of new experiments with different initial API concentrations and antisolvent flow rates (Fig. 3). The parameters of this model are given in Table 1. The current work is focused on the theoretical model-based control that is assessed in detail in the subsequent sections (Fig. 3 and Table 1).
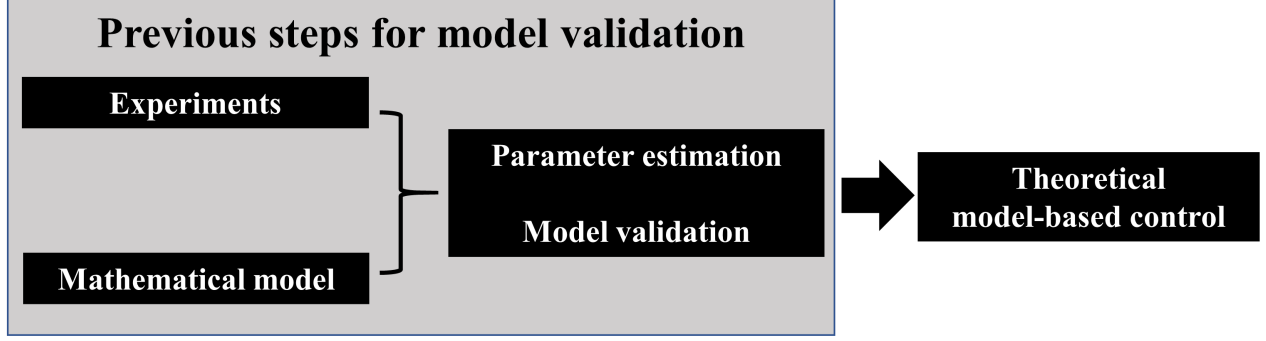
14

Figure 3: Steps needed for obtaining a validated high fidelity model for the antisolvent crystallization of aspirin in a tubular crystallizer before the theoretical model-based control is applied.[17]

Table 1: Parameters for the kinetics of crystal growth and for PI controller (Supplementary Material and[17]).

| Parameter | Nominal Value | Units | 95% Conf. Interval |
|-----------|---------------|-------|--------------------|
| $d_{in}$ | 0.002 | m | |
| $z_{max}$ | 0.500 | m | |
| $k_{j1,son}$ | $1.150 \cdot 10^{-7}$ | $\#/(\text{m}^3 \text{ s})$ | |
| $k_{j2,son}$ | 102696.000 | J/mol | 10000.000 |
| $k_{j3,son}$ | 0.16 | - | |
| $k_{G1}$ | $3.21 \cdot 10^{-4}$ | m/s | |
| $k_{G2}$ | 19652.720 | J/mol | 831.400 |
| $k_{sec,1}$ | $1.150 \cdot 10^{11}$ | $\#/(\text{m}^2 \text{ s})$ | |
| $k_{sec,2}$ | 0.0103 | - | 0.0081 |
| $K_C$ | $13.75 \cdot 10^{-8}$ | - | |
| $\tau_S$ | 10.0 | s | |
| $\tau_I$ | 15.3 | s | |

## 3.2 Step 2. Sensitivity tests and control system strategy.

Before the evaluation of the controller takes place, certain simulation sensitivity tests were necessary to be performed. Specifically, a pulse strategy was used in the sonicated crystallizer, where the manipulated variable is the volumetric flowrate of antisolvent (Fig. 4). As disturbances, the initial dissolved concentration of the API in the inlet of the crystallizer and the inlet temperature are used. Furthermore, the volumetric flow rates of solvent were considered to be constant (the output of the model is the $L_{43}$ at the outlet of the crystallizer). The profile of the pulses was chosen randomly at different volumetric flowrates of the antisolvent, and stepwise functions were used. Figs. 4.A and B show how the $L_{43}$ varies at

a low antisolvent flow rate with constant dissolved concentration of the API and constant inlet temperature, respectively. Similarly, Figs. 4.C and D show how the $L_{43}$ varies with a greater antisolvent flow rate. This strategy can capture the involved changes of the inputs in the crystallizer in a more precise way. Both the inlet temperature ($T_{in}$) and the dissolved concentration of the API in the inlet ($C_{0,in}$) indeed affect $L_{43}$. Specifically, $L_{43}$ depends on temperature because solubility changes, and both temperature and solubility have a significant effect on nucleation and growth rates after the mixing of solvent and antisolvent (Fig. 4).[17,31]
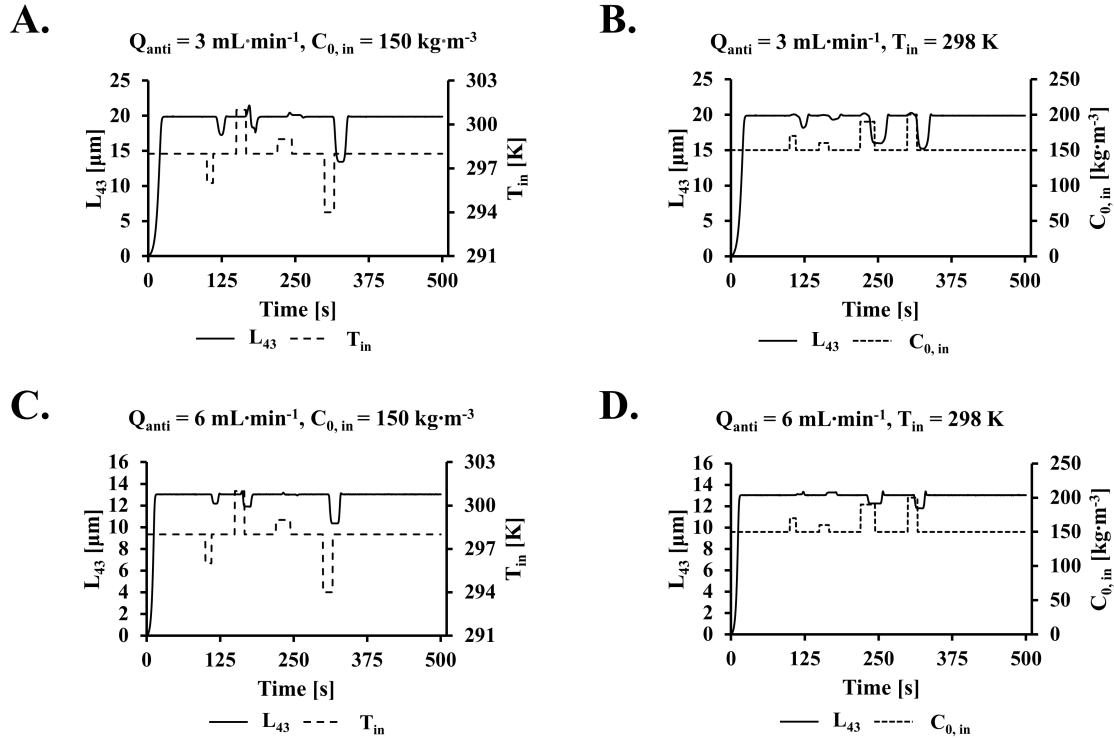


Figure 4: Pulse input strategy in the sensitivity tests (open loop simulations) for A) constant flow rate of antisolvent at 3 mL/min and constant inlet API dissolved concentration at 150 kg/m³, B) constant flow rate of antisolvent at 3 mL/min and constant inlet temperature at 298 K, C) constant flow rate of antisolvent at 6 mL/min and constant inlet API dissolved concentration at 150 kg/m³, and D) constant flow rate of antisolvent at 6 mL/min and constant inlet temperature at 298 K.

In all sensitivity tests, the cooling water temperature and the frequency of the ultrasound applied were neglected due to their insignificant effect. Specifically, the temperature in the system varies only after several minutes (>15 min) as a direct effect of cooling water

(prolonged effect). As the ultrasound frequency is of concern, it was shown that the higher the frequency, the lower the rate of generation of cavitation bubbles, which reduces the nucleation rate.[37] When the ultrasound frequency is low, small crystals are formed, in contrast to the high-frequency case. In order to apply and evaluate the proposed control system, the following actions were implemented:

- Action 1: Selection of process-controlled and manipulated variables (based on predefined targets and not through a systematic approach for this preliminary study).

- Action 2: Tuning of the applied controllers and individual evaluation of the different types (P, PI, PID).

- Action 3: Implementation of the selected (based on Step 2) type of controllers (either P, PI, or PID) and fine-tuning (if necessary).

- Action 4: Simulation of case scenarios based on realistic operation modes (Section 3.3).

Action 1: As shown in Fig. 2, a single feedback controller is utilized in the proposed system. This controller ensures that the $L_{43}$ controlled variable follows accurately the respective $(L_{43, sp})$ set-point trajectory by manipulating the volumetric flowrate of the antisolvent (MV). While not selected systematically, the applied control scheme provides a safe operation for the main system unit.

Action 2: The next step is the tuning of the applied controller via the empirical and widely known method of Ziegler – Nichols. This method is quite simple in its implementation since the controller operates as a proportional one (P-control) until the controlled variable shows oscillation of a constant magnitude. The critical gain and the critical period of oscillation $(K_{P, Crit}, T_{Crit})$ is recorded and used for the evaluation of all three P-I-D control constants according to known correlations.[38] As a typical example of tuning, the applied controller performance is shown in SI under constant oscillations. The critical gain and the critical period of oscillation is recorded, and based on these values the suitable $K_C$, $\tau_I$, $\tau_D$ controller

parameters are estimated for each candidate P, PI or PID controller, respectively. Next, simulations were performed with a P, PI and PID controller. Among them, the P controller showed expected difficulties in capturing the set-point, whereas, PI, and PID were capable of controlling the process under minimal differences.

Action 3: After tuning, the controller selected type is implemented and the dynamic response is quantitatively and qualitatively assessed. As shown in Fig. S2, the PI controller eliminates the error under an acceptable overshoot and is selected (see Table 1).

Action 4: Simulation of case scenarios based on realistic operation modes are presented and analyzed in detail in section 3.3.

## 3.3   Step 3 and 4: Case studies for feedback control and closed loop validation

In this subsection, the PI controller's implementation is based on the high fidelity model described earlier. In the studied process, a) the flow rate of the antisolvent is considered as the manipulated variable, b) the inlet temperature and the inlet concentration of the API are considered as disturbances, and c) the average volume-based mean size is the process output (controlled variable). The applied disturbances to this system can stem from the upstream process for producing the API's desired composition.

Regarding the ranges used in the inlet API dissolved concentration and inlet temperature, their values stem from previous experiments and measurements. As long as we validated our model in an antisolvent content range between 60%-90%, the inlet dissolved API concentration can vary between $150 - 200$ kg/m$^3$.[18] Also, in our previous work, we noticed that the inlet streams' temperature could show fluctuations experimentally, whereas the heat of mixing exists, as well.[17] Because the inlet solution stream could derive from an industrial process, a range of 294-301 K in the inlet temperature is reasonably assumed. For the "closed-loop" simulation, the flow rate of solvent which carries the API was kept constant at a nominal value of 2 mL/min.

The next subsections are classified into 5 different simulation cases: i) process operation under no disturbance effects, ii) process operation where disturbances occur simultaneously, iii) process operation where disturbances take place at different time instances, iv) process operation with no disturbances but with variations in the flow rate of solvent, and v) process operation with disturbances occurring at different times along with variations in the flow rate of solvent. At each different case, there are two subcategories: 1) set-point remains constant, and 2) set-point varies in time. In Figs. 5 - 9, the subfigure A shows how the disturbances vary in each case. Subfigures B1 and B2 show the $L_{43}$ when the set-point remains constant or not, respectively. In subfigures C1 and C2, the flowrate of antisolvent is presented. Overall, the last two cases of this simulation study (cases iv and v) are considered worst case scenarios as there is variation in the solvent flow rate. The small changes in the solvent flow rate allow the antisolvent content's values and the velocity to remain within the ranges of model validation.[17] Hence, all scenarios have been realistically set-up.

### 3.3.1 Case i: No disturbances

In case i where the set-point is constant (B1 and C1 from Fig. 5), the flow rate of the antisolvent (C1) increases steadily (from its nominal value) and then remains constant at 8 mL/min since the set-point for $L_{43}$ is kept constant. When the set-point varies (B2 and C2 from Fig. 5), the PI controller increases the antisolvent flow rate when smaller crystals are required. This behavior is expected since the growth rate decreases due to the low $\Delta C$. Similarly, the flow rate decreases when the set point increases due to the high $\Delta C$ (B2 and C2 from Fig. 5). Regarding $L_{43}$ (controlled variable), in both cases of set-point, $L_{43}$ reaches a steady state after 200 s, which is considered as an acceptable start-up time for this complex continuous process. The overshoot and the slight oscillatory behavior do not significantly affect the process output target during start-up. When a set-point variation is applied (B2), a quick response takes place during changes at 200 s and 400 s, and the $L_{43}$ quickly settles within the new operating targets.
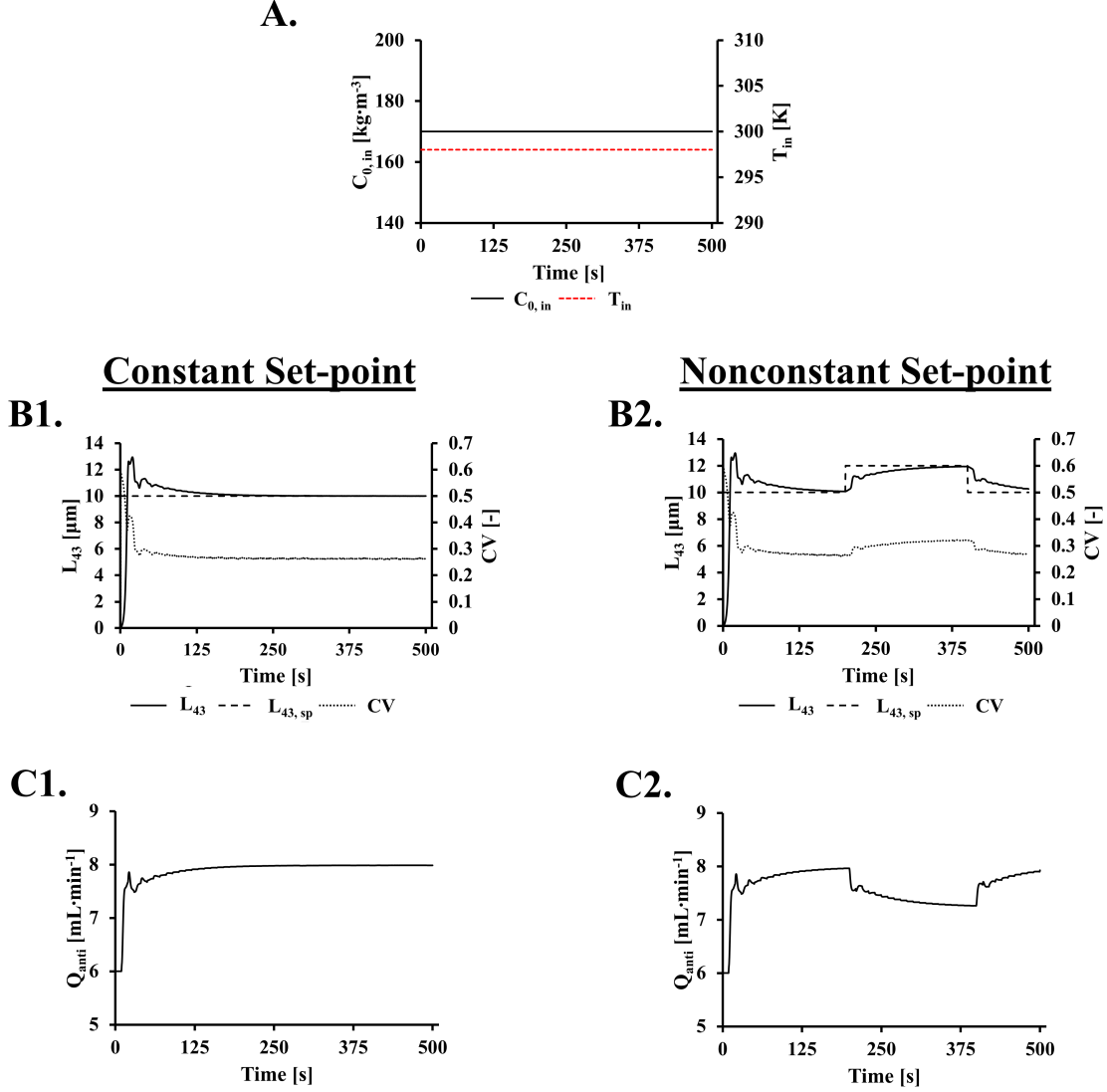
Figure 5: A) No disturbances used in the system, B1) Control of $L_{43}$ when the inlet API concentration and inlet temperature remains constant. The set-point of $L_{43}$ remains constant, and CV is estimated by Eq.21. C1) Profile of the manipulated variable. B2) Control of $L_{43}$ when the inlet API concentration and inlet temperature remain constant. The set-point of $L_{43}$ changes over time, and CV is estimated by Eq.21. C2) Profile of the manipulated variable.

### 3.3.2 Case ii: Disturbances occurring simultaneously

In this $2^{nd}$ simulation case, the following have been observed. When the set-point is constant (B1 and C1 from Fig. 6), the antisolvent flow rate records continuous variations due to disturbances that occur at different time instances of inlet concentration and temperature (see Fig. 6A). These variations affect the controlled variable of $L_{43}$ that manages however
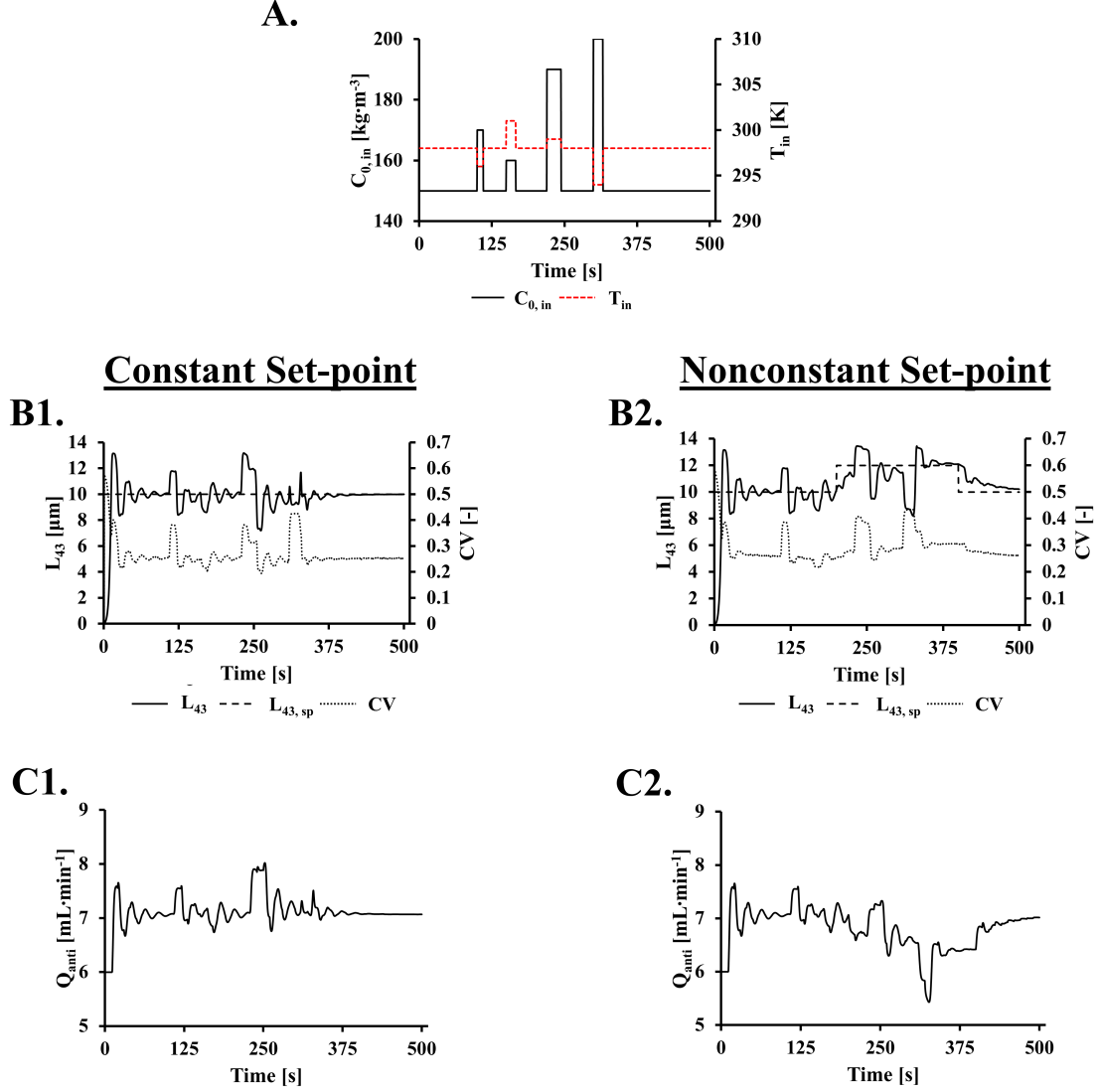
20

Figure 6: A) Simultaneously varied disturbances used in the system, B1) Control of $L_{43}$ when the inlet API concentration and inlet temperature change simultaneously. The set-point of $L_{43}$ remains constant, and CV estimated by Eq.21. C1) Profile of the manipulated variable. B2) Control of $L_{43}$ when the inlet API concentration and inlet temperature change simultaneously. The set-point of $L_{43}$ changes over time, and CV estimated by Eq.21. C2) Profile of the manipulated variable.

to stay really close to the set-point limits and with a maximum margin deviation of $\pm$ 25%. On the other hand, when set-point changes along with disturbances (B2-C2 figures), the controller manages to keep $L_{43}$ within certain limits and not allowing significant variations. The set-point settling is reasonably delayed to be achieved since disturbances occur at short time intervals.

### 3.3.3 Case iii: Disturbances occurring at different times

As Fig. 7 in B1 and C1 shows, the disturbances occurring at different time instances induce a more oscillatory behavior (as compared to Fig. 6 B1 and C1). This behavior was expected, and the controller still manages to keep $L_{43}$ really close to the set-point limits
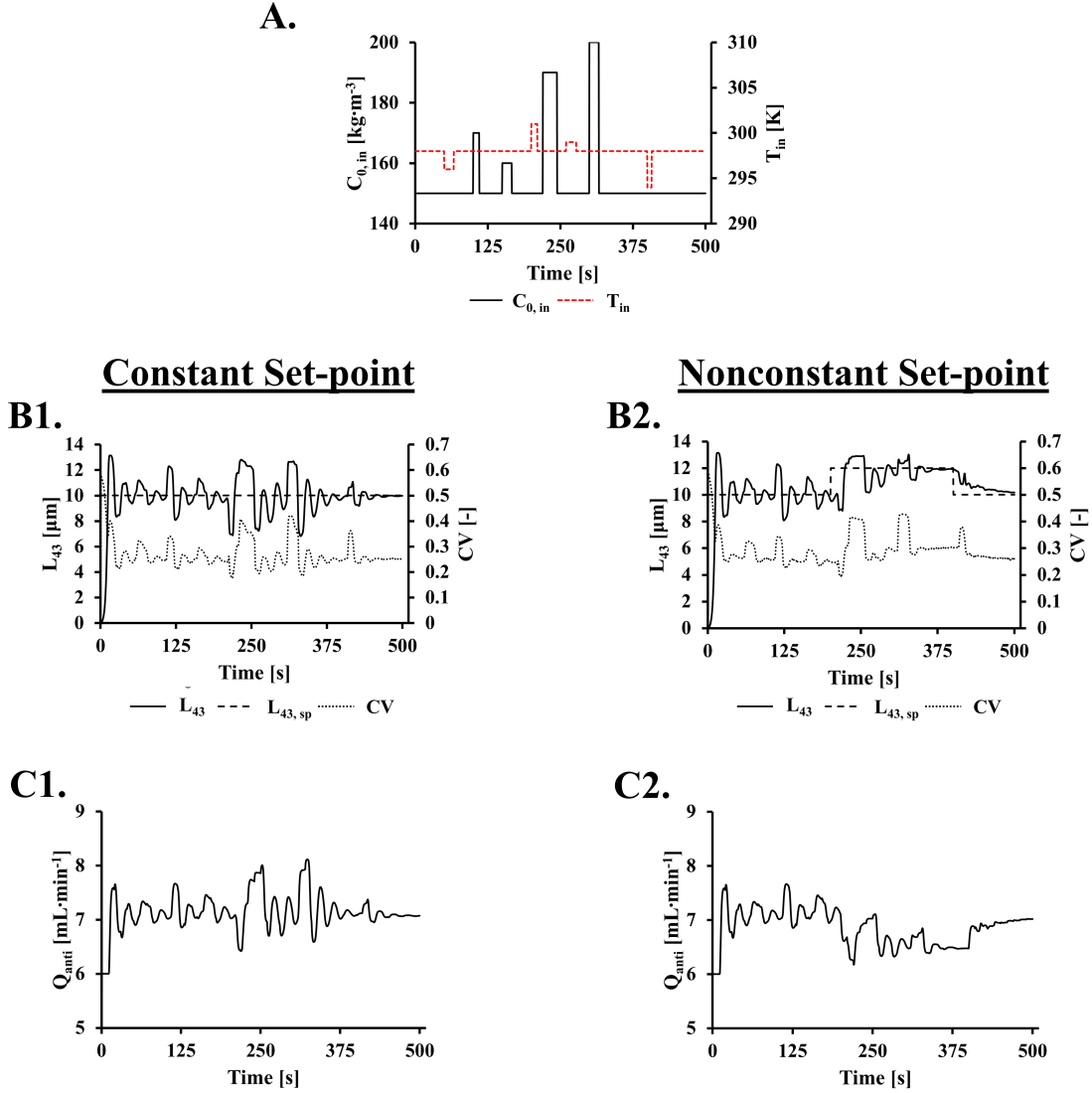


Figure 7: A) Disturbances which vary at different times used in the system, B1) Control of $L_{43}$ when the inlet API concentration and inlet temperature change at different times. The set-point of $L_{43}$ remains constant, and CV is estimated by Eq.21. C1) Profile of the manipulated variable. B2) Control of $L_{43}$ when the inlet API concentration and inlet temperature change at different times. The set-point of $L_{43}$ changes over time, and CV is estimated by Eq.21. C2) Profile of the manipulated variable.

with a maximum margin deviation of $\pm$ 25%. When the set-point varies (B2 and C2 from Fig. 7), there are slightly more harsh changes in the antisolvent flow rate. Especially, during the period 300-350 s, the PI controller decreases the antisolvent content in order to increase the $\Delta$C. This third case is the last applied simulated scenario in which only the inlet API concentration and the inlet temperature vary. The behavior of the PI controller in both cases of the set point, shows an increased flow rate of antisolvent in the durations when the inlet concentration increases, a result that was expected (B and C insets from Fig. 7).

### 3.3.4 Case iv: No disturbances and variations occurring in the flow rate of solvent

This simulation scenario's target is to assess the controller performance when the solvent flow rate suddenly varies. As shown in Fig. 8, when the solvent flow rate decreases there are simultaneous changes in the antisolvent flow rate. Specifically, the solvent decrease induces the controller to decrease the antisolvent flow rate. What is noticeable is the fact that while the increase of the solvent flow rate does not induce significant variations, it is the solvent decrease that produces significant changes to the antisolvent flow at 160 - 190 s and 300 - 350 s in (C1) and (C2) of Fig. 8, respectively. During these periods, the PI controller adjusts the antisolvent content in order to increase the inlet concentration of the API (this result causes the production of smaller crystals). This $4^{th}$ case is the first worst case in which there are no disturbances in the inlet API concentration and the inlet temperature, but the solvent flow rate varies significantly. The PI controller's behavior in both set-point cases shows a desired trend as long as large crystals maintain an acceptable size (B and C insets from Fig. 8).

### 3.3.5 Case v: Disturbances at different times with variations in flow rate of solvent

In this last scenario, several distorting disturbances take place (Fig. 9). The antisolvent flow rate performs continuous variations due to these disturbances occurring at different
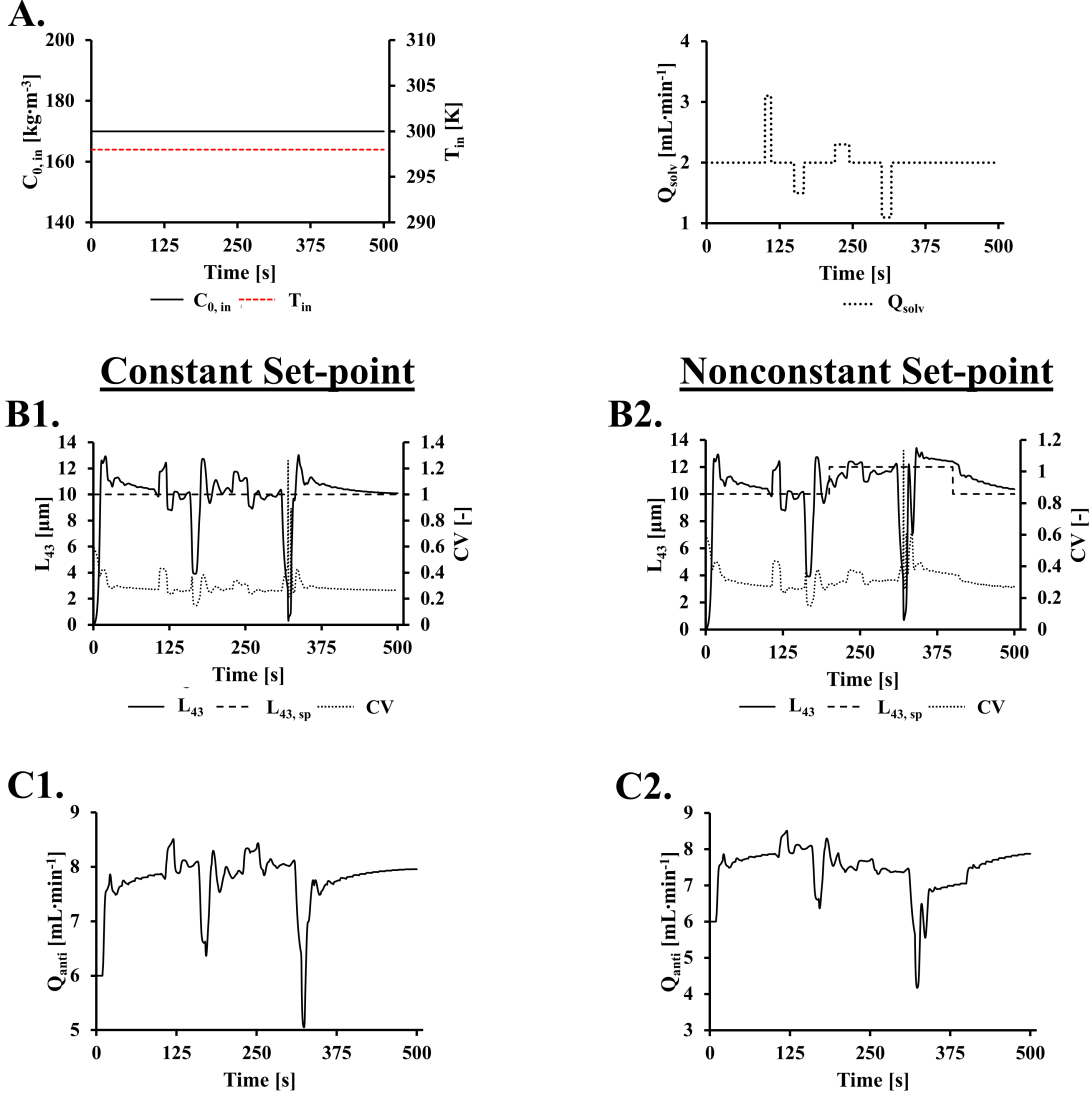
Figure 8: A) No disturbances are used in the system (left), but the flow rate of solvent varied over time (right), B1) Control of $L_{43}$ when the inlet API concentration and inlet temperature do not change except the solvent flowrate. The set point of $L_{43}$ remains constant, and CV is estimated by Eq.21. C1) Profile of the manipulated variable. B2) Control of $L_{43}$ when the inlet API concentration and inlet temperaturedo not change except the solvent flowrate. The set point of $L_{43}$ changes over time, and CV is estimated by Eq.21. C2) Profile of the manipulated variable.

time instances. These overall variations affect the controlled variable of $L_{43}$ which manages however to keep close to the set-point limits despite this detrimental operating pattern. This case scenario while being rather unrealistic, still shows significant insights on the well-tuned controller. If a badly-tuned controller was designed and applied, then the controlled variable's
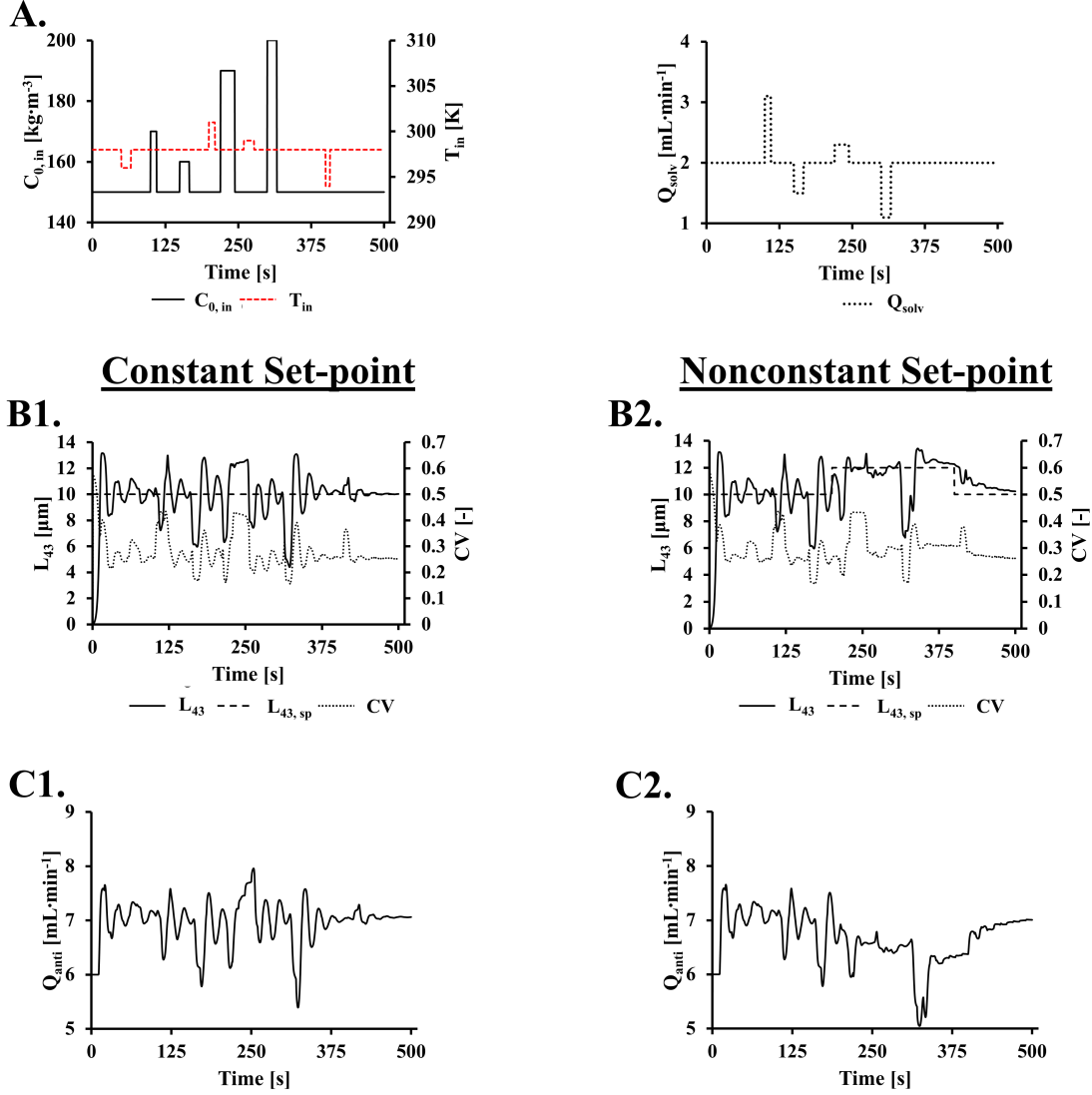
Figure 9: A) Disturbances that vary at different times used in the system (left), and the flow rate of solvent varied over time as well (right), B1) Control of $L_{43}$ when the inlet API concentration, inlet temperature, and the solvent flowrate change at different times. The set-point of $L_{43}$ remains constant, and CV is estimated by Eq.21. C1) Profile of the manipulated variable. B2) Control of $L_{43}$ when the inlet API concentration, inlet temperature, and the solvent flowrate change at different times. The set-point of $L_{43}$ changes over time, and CV is estimated by Eq. 21. C2) Profile of the manipulated variable.

overall profile $L_{43}$ would be detrimental for the studied process. The set-point is reasonably delayed to be achieved because disturbances occur at short time intervals something that could happen in realistic scenarios. As shown in Tables 2 and 3, the $L_{43}$ reaches the set-point with some small variations at 10 $\mu m$ for all applied scenarios. The average size of all crystals

collected with constant (Table 2) and varied set-point (Table 3) in the beaker are small, close to the set-point and their correlation distribution is narrow (CV 0.30).

Table 2: Quality of collected crystals in the outlet in cases from i to v when the set point remains constant.

| Case | $L_{43,col.}$ [$\mu$m] | $CV_{col.}$[-] |
|------|------------------------|----------------|
| i    | 10.05                  | 0.28           |
| ii   | 9.81                   | 0.27           |
| iii  | 9.90                   | 0.27           |
| iv   | 9.98                   | 0.29           |
| v    | 9.80                   | 0.28           |

Table 3: Quality of collected crystals in the outlet in cases from i to v when the set point changes over time.

| Case | | 0 - 200 s | 200 - 400 s | 400 - 500 s |
|------|--------------------------|-----------|-------------|-------------|
| i    | $L_{43,col.}$[$\mu m$]    | 10.09     | 11.59       | 10.72       |
|      | $CV_{col.}$[$-$]         | 0.29      | 0.31        | 0.28        |
| ii   | $L_{43,col.}$[$\mu m$]    | 9.60      | 11.54       | 10.70       |
|      | $CV_{col.}$[$-$]         | 0.28      | 0.32        | 0.27        |
| iii  | $L_{43,col.}$[$\mu m$]    | 9.7       | 11.64       | 10.63       |
|      | $CV_{col.}$[$-$]         | 0.29      | 0.31        | 0.28        |
| iv   | $L_{43,col.}$[$\mu m$]    | 9.84      | 11.25       | 11.00       |
|      | $CV_{col.}$[$-$]         | 0.31      | 0.35        | 0.29        |
| v    | $L_{43,col.}$[$\mu m$]    | 9.51      | 11.51       | 10.77       |
|      | $CV_{col.}$[$-$]         | 0.30      | 0.31        | 0.28        |

## 3.4   Overview and Discussion

From an in silico point of view, particle size control can be achieved by controlling the anti-solvent flow rate at the application of ultrasound. During the application of the ultrasound, the cavitation caused is responsible for attrition and breakage effects in the crystals, decreasing the size of the produced crystals.[39,40] Our system's initial sensitivity tests helped to identify the experimental conditions that have the most significant impact on specific outputs like the $L_{43}$. These tests showed that the inlet temperature is more responsible for the crystal growth because both nucleation and growth rates depend on the solubility,

which is a function of temperature and the antisolvent content in the studied process (see Fig. 4). When the concentration is high, the supersaturation ratio increases and affects the size of the produced crystals.[41] More specifically, the nucleation rate increases at higher supersaturation ratios, and smaller crystals appear due to the increased number of nuclei.[17] If we compare our produced crystals under control with the crystal sizes obtained without control, it is observed that the control allowed us to obtain crystals with smaller average size, and narrower coefficient of variation of crystals' population.[17]

From an experimental point of view, the online crystal characterization can be achieved by the use of a high speed camera. Crystals produced are suspended homogeneously in the moving fluid. The crystals then pass through a thin flow cell in the optical path during their movement. A beam of light passes through the flow cell as well, thus projecting the particles' images onto a high-resolution camera sensor. The combination of the high frame rate with the high resolution of the camera and a high-speed host computer achieves the characterization of a huge number of crystals per second in real-time. Apart from the diameter, this method is ideal for applications where the shape is important for predicting raw material performance.[21,22]

In our experimental setup, it is assumed that there is a high speed camera that provides information about the crystal size distribution to the controller each 10 s. The sampling time is selected based on the residence time distribution in the milifluidic device. Therefore, based on the error between the set-point and the measured value at the output, the PI controller controls the antisolvent flow rate. Temperature control from cooling water was not tested in this study, whereas, the frequency and the power of the ultrasound transducer remain constant. The former belongs to a range of frequencies where the crystals produced are small and sizes do not vary significantly when frequency varies within the small range.[42] The latter does not affect the cavitation and shows higher yield when it decreases because there is less temperature increase at lower powers.[18]

Regarding our proposed controller scheme, the selected PI controller was initially coupled

in our high fidelity model. The case studies used are likely to appear during the crystallization of an upstream process. Disturbances might not be obvious in ideal conditions, but they can occur either together or at different time periods. The ranges used in the inlet temperature and API concentration stem from previous studies.[17,18] Furthermore, disturbances in the flow rate of solvent were added and assumed as extreme cases, as these disturbances might rarely appear in the real process. Both the inlet temperature and inlet API concentration affect the nucleation, the growth rate, and the solubility. Thus, the PI controller's main action was to figure out how the antisolvent flow rate should vary, so that the system's conditions will allow the production of crystals with the desired size. When there is a high dilution from the antisolvent, it is worth noticing that the growth rate might be negligible due to the fact that the API concentration decreases and solubility decreases too ($\Delta C \approx 0$).

Regarding the quality of the crystals collected, Table 2 showed the average collected size and the CV of the crystals when the set-point remains constant or not, respectively. When the set-point remained constant, the beaker's collected crystals had an average crystal size 10 $\mu$m and a CV value less than 0.30 (Table 2). These values denote that not only the crystal population collected will have the desired size, but also the range of their crystal size distribution will be quite narrow. When the set-point varied (Table 3), the same collected values of $L_{43}$ and CV were obtained. Some durations caused the CV values to be larger than 0.30; such issues can be assumed reasonable, as long as the system is tested under extreme and unexpected conditions.

Overall, this study proved that a conventional feedback control scheme can be implemented at the ultrasound-assisted continuous antisolvent crystallization of aspirin. The simulated cases involving a series of emerged disturbances are especially representative of the excellent controller tuning. Clearly, such a behavior simulates worst-case scenarios and hence, the unit operation's real performance is expected to lead to even higher quality crystals. As a future step, this research group aims to discuss the application of modern control schemes such as Model Predictive Control (MPC). MPC is continuously applied in vari-

ous industrial processes (mainly in refineries) and possesses the advantage of optimizing the manipulated variable sequence towards minimum set-point deviations. To this end, the process's economics will be reduced (less effort from the manipulated variable) even further, which is clearly the key to move to larger-scale production rates. Based on this advanced approach, the future implementation of a proposed MPC scheme would intake the exact same manipulated and controlled variables as with the conventional PI controller and include as an objective function: a) the squared error of the controlled variable from the predefined set-point signal and b) the squared error of the manipulated variable from its steady-state point. In this way, the MPC scheme will not only minimize the operating error, but also maintain the volumetric flowrate of the antisolvent within certain limits that will significantly improve the continuous crystallization process economics. Similar studies have already been found to lead to a significant improvement on the batch crystallization process[43,44] and on continuous manufacturing processes.[45]

# 4    Conclusions

Controlling the ultrasound-assisted antisolvent crystallization of aspirin from ethanol/water in a continuous tubular crystallizer was analyzed theoretically in this study. It was shown that the system could produce small crystal sizes with a more narrow crystal size distribution. During controller assessment, the system was validated mathematically, as long as, the crystal sizes and their distributions were studied at different experimental conditions (flow rates and API initial concentrations). Empirical and verified expressions were employed in the estimation of the controller parameters (Ziegler-Nichols tuning methodology). The coupling of the controller with the high fidelity model allowed the process to find the profile of the manipulated variable that captured the desired set-point at different disturbances. The disturbances applied to the studied system are possible to occur, as the system has been previously studied experimentally. Applying the disturbances in our system, the controller

can manipulate the antisolvent flow rate efficiently for producing crystals whose $L_{43}$ set-point is 10 $\mu$m or 12 $\mu$m with a narrow CV which approximates to 0.30. This work is practical in that (1) disturbances' profiles used in our system have been obtained from experimental experience, (2) from kinetics' data that are readily available in the literature, (3) it finds the experimental conditions that control the crystal growth along the crystallizer, and (4) it produces the crystal with small sizes and narrow distributions. The controller used in this work should be evaluated for the scale-up of continuous crystallizers to industrially relevant throughputs and with more advanced process control schemes.

# Acknowledgements

# Abbreviations

ASA, Acetyl-Salicylic acid, Aspirin

API, Active Pharmaceutical Ingredient

MOMs, Method of Moments

MPC, Model Predictive Control

MSMPR, Mixed-Suspension, Mixed-Product Removal

P, Proportional Controller

PBM, Population Balance Models

PI, Proportional Integral Controller

PID, Proportional Integral Derivative Controller

PSD, Particle Size Distribution

# Symbols

$a_c$, heat transfer area per unit volume, [m$^2$/m$^3$]

$B_{son}$, nucleation rate from ultrasound, [#/(m$^3$ s)]

$C$, API concentration in the solution, [kg/m$^3$]

$C_0$, initial API concentration in the crystallizer, [kg/m$^3$]

$C_{0,in}$, initial API concentration in the inlet, [kg/m$^3$]

$C_{feed}$, inlet API concentration, [kg/m$^3$]

$C_{sat}$, solute solubility, [kg/kg]

$CV$, coefficient of variation, [-]

$C_w$, API concentration, [kg/kg]

$Cp$, specific heat capacity of the mixture, [J/(kg K) ]

$d_{in}$, inner diameter of the tubular crystallizer, [m]

$e$, error, [m]

$G$, crystal growth rate, [m/s]

$k_{G1}$, empirical parameter in growth rate, [m/s]

$k_{G2}$, empirical parameter in growth rate, [J/mol]

$k_{j1,son}$, empirical parameter in nucleation rate, [#/(m$^3$ s)]

$k_{j2,son}$, empirical parameter in nucleation rate, [J/mol]

$k_{j3,son}$, empirical parameter in nucleation rate, [-]

$k_{sec,1}$, empirical parameter in nucleation rate, [#/(m$^2$ s)]

$k_{sec,2}$, empirical parameter in nucleation rate, [-]

$K_c$, proportional term, [-]

$K_v$, volume shape factor, [-]

$L$, crystal size, [m]

$L_0$, the nuclei size, [m]

$L_{43}$, volume-based mean crystal size, [m]

$L_{43,sp}$, set-point of the volume-based mean crystal size, [m]

$n$, crystal number density, $[\#/(\text{m}^3 \text{ m})]$

$n_0$, initial number probability density function for the PSD, $[\#/(\text{m}^3 \text{ m})]$

$n_{feed}$, the crystal size distribution at the inlet of the crystallizer, $[\#/(\text{m}^3 \text{ m})]$

$n_L$, number of discretized bins along the crystal size ($L$- axis), [-]

$n_z$, number of discretized bins along the crystallizer's length ($z$- axis), [-]

$P$, overall control function, [-]

$P_{net,cal}$, calorimetric ultrasound power, $[\text{J}/(\text{m}^3 \text{ s})]$

$P_{net,US}$, applied power of ultrasound, $[\text{J }/\text{s}]$

$Q_{anti}$, volume flow rate of antisolvent, $[\text{m}^3/\text{s}]$

$Q_{solv}$, volume flow rate of solvent and solute, $[\text{m}^3/\text{s}]$

$R$, ideal gas constant, $[\text{J}/(\text{mol K})]$

$S$, supersaturation ratio, [-]

$t$, time, [s]

$T$, temperature of the mixture, [K]

$T_{in}$, inlet temperature of the mixture, [K]

$T_0$, initial temperature of the mixture in the crystallizer, [K]

$T_w$, temperature of the cooling water, [K]

$u_z$, velocity of the slurry, [m/s]

$U_c$, overall heat transfer coefficient, $[\text{J}/(\text{m}^2 \text{ s K}) ]$

$w$, antisolvent content, [-]

z, z- coordinate

$z_{max}$, maximum crystallizer length, [m]

$\Delta H_{mix}$, enthalpy of mixing, [J/kg]

$\Delta H_{crys}$, heat of crystallization, $[\text{W}/\text{m}^3]$

$\rho$, mixture density, $[\text{kg}/\text{m}^3]$

$\rho_c$, crystal density, $[\text{kg}/\text{m}^3]$

$\tau_D$, derivative time, [s]

$\tau_I$, integral time, [s]

# Supporting Information Available

The following files are available free of charge.

The Supplementary Material contains details about the controller tuning. Three different controllers are used: i) a proportional (P) controller, ii) a proportional integral (PI) controller, and iii) a proportional integral derivative (PID) controller.

# References

(1) Gao, Z.; Rohani, S.; Gong, J.; Wang, J. Recent developments in the crystallization process: Toward the pharmaceutical industry. *Engineering* **2017**, *3*, 343–353.

(2) Wu, K.-L.; Wang, H.-Y.; Ward, J. D. Economic comparison of crystallization technologies for different chemical products. *Ind. Eng. Chem. Res.* **2018**, *57*, 12444–12457.

(3) Yang, X.; Acevedo, D.; Mohammad, A.; Pavurala, N.; Wu, H.; Brayton, A. L.; Shaw, R. A.; Goldman, M. J.; He, F.; Li, S.; Fisher, R. J.; O'Connor, T. F.; Cruz, C. N. Risk considerations on developing a continuous crystallization system for carbamazepine. *Org. Process Res. Dev.* **2017**, *21*, 1021–1033.

(4) McGinty, J.; Chong, M. W.; Manson, A.; Brown, C. J.; Nordon, A.; Sefcik, J. Effect of process conditions on particle size and shape in continuous antisolvent crystallisation of lovastatin. *Crystals* **2020**, *10*, 925.

(5) Raber, I.; McCarthy, C. P.; Vaduganathan, M.; Bhatt, D. L.; Wood, D. A.; Cleland, J. G.; Blumenthal, R. S.; McEvoy, J. W. The rise and fall of aspirin in the primary prevention of cardiovascular disease. *The Lancet* **2019**, *393*, 2155–2167.

(6) Zamanipoor, M. H.; Mancera, R. L. The emerging application of ultrasound in lactose crystallisation. *Trends Food Sci Technol* **2014**, *38*, 47–59.

(7) Dodds, J.; Espitalier, F.; Louisnard, O.; Grossier, R.; David, R.; Hassoun, M.; Baillon, F.; Gatumel, C.; Lyczko, N. The effect of ultrasound on crystallisation-precipitation processes: Some examples and a new segregation model. *Part. Part. Syst. Charact.* **2007**, *24*, 18–28.

(8) Fernandez Rivas, D.; Kuhn, S. Synergy of Microfluidics and Ultrasound. *Top. Curr. Chem.* **2016**, *374*, 70–99.

(9) Kiss, A. A.; Geertman, R.; Wierschem, M.; Skiborowski, M.; Gielen, B.; Jordens, J.; John, J. J.; Van Gerven, T. Ultrasound-assisted emerging technologies for chemical processes. *J. Chem. Technol. Biotechnol.* **2018**, *93*, 1219–1227.

(10) Fatemi, N.; Dong, Z.; Van Gerven, T.; Kuhn, S. Microbubbles as heterogeneous nucleation sites for crystallization in continuous microfluidic devices. *Langmuir* **2018**, *35*, 60–69.

(11) Eder, R. J.; Schrank, S.; Besenhard, M. O.; Roblegg, E.; Gruber-Woelfler, H.; Khinast, J. G. Continuous sonocrystallization of acetylsalicylic acid (ASA): Control of crystal size. *Cryst. Growth Des.* **2012**, *12*, 4733–4738.

(12) Tokuhisa, T.; Kawasaki, M.; Kisailus, D.; Yuda, M.; Matsunaga, T.; Arakaki, A. Crystal Growth of Aspirin Using a Temperature-Controlled Microfluidic Device. *Cryst. Growth Des.* **2015**, *15*, 4549–4555.

(13) Nagy, Z. K.; Fevotte, G.; Kramer, H.; Simon, L. L. Recent advances in the monitoring, modelling and control of crystallization systems. *Chem. Eng. Res. Des.* **2013**, *91*, 1903–1922.

(14) Fujiwara, M.; Nagy, Z. K.; Chew, J. W.; Braatz, R. D. First-principles and direct design approaches for the control of pharmaceutical crystallization. *J. Process Control* **2005**, *15*, 493–504.

(15) Kwon, J. S.-I.; Nayhouse, M.; Orkoulas, G.; Christofides, P. D. Crystal shape and size control using a plug flow crystallization configuration. *Chem. Eng. Sci.* **2014**, *119*, 30–39.

(16) Diab, S.; Gerogiorgis, D. I. No More Than Three: Technoeconomic Mixed Integer Nonlinear Programming Optimization of Mixed Suspension, Mixed Product Removal Crystallizer Cascades for Melitracen, an Antidepressant API. *Ind. Eng. Chem. Res.* **2020**, *59*, 21458–21475.

(17) Savvopoulos, S. V.; Hussain, M. N.; Jordens, J.; Waldherr, S.; Van Gerven, T.; Kuhn, S. A Mathematical Model of the Ultrasound-Assisted Continuous Tubular Crystallization of Aspirin. *Cryst. Growth Des.* **2019**, *19*, 5111–5122.

(18) Hussain, M. N.; Jordens, J.; John, J.; Braeken, L.; Van Gerven, T. Enhancing pharmaceutical crystallization in a flow crystallizer with ultrasound: Anti-solvent crystallization. *Ultrason. Sonochem.* **2019**, *59*, 104743.

(19) Zhang, D.; Xu, S.; Du, S.; Wang, J.; Gong, J. Progress of pharmaceutical continuous crystallization. *Engineering* **2017**, *3*, 354–364.

(20) Ramkrishna, D. *Population balances: Theory and applications to particulate systems in engineering*; Academic Press: San Diego, CA, 2000; pp 7–46.

(21) Deguchi, K. An image processing technique for high-speed measurement of particle-size distributions. *Measurement* **1986**, *4*, 128–133.

(22) Friese, C. A.; van der Does, M.; Merkel, U.; Iversen, M. H.; Fischer, G.; Stuut, J.-B. W.

Environmental factors controlling the seasonal variability in particle size distribution of modern Saharan dust deposited off Cape Blanc. *Aeolian research* **2016**, *22*, 165–179.

(23) Su, Q.; Benyahia, B.; Nagy, Z. K.; Rielly, C. D. Mathematical modeling, design, and optimization of a multisegment multiaddition plug-flow crystallizer for antisolvent crystallizations. *Org. Process Res. Dev.* **2015**, *19*, 1859–1870.

(24) Fluorotherm: Ultrapure shell and tube heat exchanger. `https://www.fluorotherm.com/wp-content/uploads/2014/04/UltrapureShellAndTubeHeatExchanger.pdf`, Accessed: 2018-09-30.

(25) Lemmon, E. W.; Bell, I.; Huber, M. L.; McLinden, M. O. NIST Standard Reference Database 23: Reference Fluid Thermodynamic and Transport Properties-REFPROP, Version 10.0, National Institute of Standards and Technology. 2018; `https://www.nist.gov/srd/refprop`.

(26) Danahy, B.; Minnick, D.; Shiflett, M. Computing the composition of ethanol-water mixtures based on experimental density and temperature measurements. *Fermentation* **2018**, *4*, 72–78.

(27) da Rosa, C. A.; Braatz, R. D. Multiscale modeling and simulation of macromixing, micromixing, and crystal size distribution in radial mixers/crystallizers. *Ind. Eng. Chem. Res.* **2018**, *57*, 5433–5441.

(28) Peeters, D.; Huyskens, P. Endothermicity or exothermicity of water/alcohol mixtures. *J. Mol. Struct.* **1993**, *300*, 539–550.

(29) Schall, J. M.; Mandur, J. S.; Braatz, R. D.; Myerson, A. S. Nucleation and growth kinetics for combined cooling and antisolvent crystallization in a mixed-suspension, mixed-product removal system: Estimating solvent dependency. *Cryst. Growth Des.* **2018**, *18*, 1560–1570.

(30) Bari, A. H.; Pandit, A. B. Sequential crystallization parameter estimation method for determination of nucleation, growth, breakage, and agglomeration kinetics. *Ind. Eng. Chem. Res.* **2018**, *57*, 1370–1379.

(31) Lindenberg, C.; Krättli, M.; Cornel, J.; Mazzotti, M.; Brozio, J. Design and optimization of a combined cooling/antisolvent crystallization process. *Cryst. Growth Des.* **2008**, *9*, 1124–1136.

(32) Gao, Y.; Lakerveld, R. Gain scheduling PID control for directed self-assembly of colloidal particles in microfluidic devices. *AIChE J.* **2019**, *65*, e16582.

(33) Ipsakis, D.; Damartzis, T.; Papadopoulou, S.; Voutetakis, S. Dynamic Modeling and Control of a Coupled Reforming/Combustor System for the Production of H2 via Hydrocarbon-Based Fuels. *Processes* **2020**, *8*, 1243.

(34) Jha, S.; Karthika, S.; Radhakrishnan, T. Modelling and control of crystallization process. *Resource-Efficient Technologies* **2017**, *3*, 94–100.

(35) Fadali, M. S.; Visioli, A. Digital control engineering. *Analysis and design* **2013**,

(36) PSE, *gPROMS Advanced User Guide*; Process Systems Enterprise: London, UK, 2004; pp 37–65.

(37) Jordens, J.; Gielen, B.; Braeken, L.; Van Gerven, T. Determination of the effect of the ultrasonic frequency on the cooling crystallization of paracetamol. *Chem. Eng. Process.* **2014**, *84*, 38–44.

(38) Åström, K. J.; Hägglund, T. *PID controllers: theory, design, and tuning*; Instrument society of America Research Triangle Park, NC, 1995; Vol. 2.

(39) Ramisetty, K. A.; Pandit, A. B.; Gogate, P. R. Ultrasound-assisted antisolvent crystallization of benzoic acid: Effect of process variables supported by theoretical simulations. *Ind. Eng. Chem. Res.* **2013**, *52*, 17573–17582.

(40) Rasche, M. L.; Zeiger, B. W.; Suslick, K. S.; Braatz, R. D. Mathematical modelling of the evolution of the particle size distribution during ultrasound-induced breakage of aspirin crystals. *Chem. Eng. Res. Des.* **2018**, *132*, 170–177.

(41) Jordens, J.; Canini, E.; Gielen, B.; Van Gerven, T.; Braeken, L. Ultrasound assisted particle size control by continuous seed generation and batch growth. *Crystals* **2017**, *7*, 195–214.

(42) Jordens, J.; Appermont, T.; Gielen, B.; Van Gerven, T.; Braeken, L. Sonofragmentation: Effect of ultrasound frequency and power on particle breakage. *Cryst. Growth Des.* **2016**, *16*, 6167–6177.

(43) Nayhouse, M.; Tran, A.; Kwon, J. S.-I.; Crose, M.; Orkoulas, G.; Christofides, P. D. Modeling and control of ibuprofen crystal growth and size distribution. *Chem. Eng. Sci.* **2015**, *134*, 414–422.

(44) Curitiba Marcellos, C. F.; Durand, H.; Kwon, J. S.-I.; Gomes Barreto Jr, A.; Laranjeira da Cunha Lage, P.; Bezerra de Souza Jr, M.; Secchi, A. R.; Christofides, P. D. Optimal operation of batch enantiomer crystallization: From ternary diagrams to predictive control. *AIChE J.* **2018**, *64*, 1618–1637.

(45) Wu, Q.; Du, W.; Nagy, Z. Steady-state target calculation integrating economic optimization for constrained model predictive control. *Comput. Chem. Eng* **2021**, *145*, 107145.